ARCHIVES OF ACOUSTICS
28, 2, 109—116 (2003)

PHASED ARRAY OPTIMIZING CHARACTERISTICS IN HIFU DEVICE

QI CHEN, BIN XIONG and YAZHU CHEN

Department of Biomedical Engineering, Shanghai JiaoTong University,
Shanghai, 200030, P. R. China

For the high intensity focused ultrasound (HIFU) phased array, frequency, distribution pattern, size and amount of the elements may affect the performance and cost of the HIFU device. In this paper an inner holed spherical shell with 96 transducer elements was designed basing on the Ebbini pseudo-inverse matrix and Penns bioheat transfer equation. The phased array has a lower grating-lobe level and a higher intensity gain suitable for deep heating. The experiments with the array using 16 elements show that the phased array design produces a large dynamic scan scale with least elements and a high heat focus.

Key words: focused ultrasound; phased array; bioheat transfer; optimization.

1. Introduction

HIFU has been used as a noninvasive treatment of localized deep diseased tissue [1,2]. HIFU of phased array has advantage over the traditional physical focus because of the complexity of the devices and reliability of the focus [3]. The random [4] and annular arrays [5] have the ability to build a high intensity focus. But excessive array elements will make the HIFU device too bulky and complicate to be fulfilled. Rational array patterns can solve the contradictions to a certain extent, e.g., a spherical-section array produced a higher intensity gain than a planar one with the same array element size and number, and the array with unequal distant elements made smaller lobes than the array with equal distant elements [6,7].

Phased arrays are able to focus the ultrasound electronically in the tumor's sagittal plane. A rational parameter choice of the phased arrays, such as frequency, size, the number, distribution patterns of elements and curvature of the spherical shell array, can increase the focusing performance and reduce the cost of the HIFU device. In this paper we studied an algorithm to produce optimal arrays with least elements, a large dynamic scan scale and an eligible grating lobe level based on the Ebbini pseudo-inverse algorithm [8] and the Pennes equation [9]. Power is supplied to the array elements from a signal driving system based on FPGA (Field Programmable Gate Array), which provides multi-channel precise phased signals with 5.625° phase shift resolution from 0 to 360° for the HIFU device.

2. Optimizing methods

The thermal response of the tissue under the ultrasound exposure is governed by Pennes bioheat transfer equation

$$\rho C_t \frac{\partial T}{\partial t} = K\nabla^2 T + \omega C_b (T_a - T) + Q_m + Q_v \tag{1}$$

where ρ, C and K are the density, specific heat and thermal conductivity with subscripts b and t referring respectively to the blood and tissue domain, T_a is the artery temperature, ω is perfusion rate, Q_m is the metabolic energy generation, Q_v is the tissue SAR (Specific Absorption Rate) of the ultrasound energy.

The main purpose of the HIFU treatment is to build a proper SAR distribution in the target tissue. The power deposition at position $r_m = (x, y, z)$ relates to the ultrasound pressure p and the tissue absorption coefficient α_α at this point.

$$q_v(r_m) = 2\alpha_\alpha \frac{p(r_m)p^*(r_m)}{\rho c} \tag{2}$$

where c is the sound velocity in the tissue, and $\alpha_\alpha = \alpha_{\alpha 0} f^i$, $\alpha_{\alpha 0}$ and i are the constants varying with different tissues.

The Ebbini pseudo-inverse algorithm is used for computing the driving amplitudes and phases of array elements from the sound pressure distribution

$$\mathbf{u} = \mathbf{H}^+ \mathbf{p} \tag{3}$$

where $\mathbf{u} = [u_1, u_2, \Lambda, u_N]^t$ is the vector of the complex surface velocity of N elements, $\mathbf{p} = [p_1, p_2, \Lambda, p_M]^t$ is the sound pressure vector of M control points, $\mathbf{H}^+$ is the pseudo-inverse of the $M \times N$ matrix $\mathbf{H}$. The element of matrix $\mathbf{H}$ is h_{mn} and is equal to

$$h_{mn} = jf\rho \iint_{S_n} \frac{e^{-jkr_{mn}} e^{-\alpha d}}{r_{mn}} ds_n \tag{4}$$

where r_{mn} is the distance from the sound pressure point r_m to the incremental source area of the complete n-th transducer element area s_n, $k = 2\pi/\lambda$ is the wave number, λ is the ultrasonic wavelength, α is the attenuation coefficient in the lossy material, and d is the ray distance in the lossy material between the source point and the location of the desired pressure point.

For a homogeneous tissue, combining (2) with (3) results in the relation between $\mathbf{u}$ and Q_v

$$\mathbf{u} = \mathbf{H}^{+} (A \cdot \mathbf{Q}_v) \tag{5}$$

where $A = \sqrt{\rho c / \alpha_\alpha}$, $\mathbf{Q}_v = [\sqrt{q_{v1}}, \sqrt{q_{v2}} \Lambda \sqrt{q_{vM}}]'$. In this way, the relationship between the ultrasound field and the driving signals was extended to the relationship between the SAR and the driving signals.

3. Results and discussion

The purpose of the optimization procedure is to find the array with rational element distribution patterns and design parameters, such as frequency, the element size and curvature of the spherical shell, in order to achieve the desired Q_v and eligible lobe level in the expected target scale with a least element number.

$$\begin{cases} J = \min\limits_{f,R,d_e} N, \text{ such that } \mathbf{Q}_v = A_1; \\ p_m = \max\limits_{n=1,2,\Lambda N} \left(\dfrac{\rho c}{2} \left| u_n \right|^2 \right) \le A_2; \\ d_{ee} / \lambda \le A_3 \end{cases} \tag{6}$$

where A_1, A_2, and A_3 are SAR for a single focus, sound intensity of the element, and ratio of the distance between the element centers to the sound wavelength. R is the spherical shell radius, d_e is the circle element diameter, d_{ee} is the smallest central distance between adjacent elements, ideally $d_e = d_{ee}$ avoiding great array aperture. For different treatment targets, different scan scale requirements, different transducer material, and different element distribution arrays, different values may be determined for A_1, A_2, and A_3.

Specific steps of the algorithm are as follows:

- Determine the treatment aims, such as A_1, D_1, D_2, D_3 and D_4 in Fig. 1.
- Choose array pattern and define A_3 and D_5 that can ensure that no excessive lobes are present.
- Define a smaller or the smallest value of N.
- Find $\min\limits_{f,R,d_e} \mathbf{u} = \mathbf{H}^{+} (A \cdot \mathbf{Q}_v)$ under the defined N.
- Judge whether $p_m \le A_2$; If no, $N = N + 1$, then go to step •; If yes, give the result f, R, d_e and N and finish the optimization.

Using the above algorithm, an inner holed spherical shell array containing circle elements was designed, as shown in Fig. 2. The treatment aims and optimization results are described in Table 1, and the tissue thermal properties [10] are used in calculations. Figure 3 (a) and (b) are the x-y axis and the side elevation acoustic field when the phased array produces a focus with 100W/cm^2 intensity in (0, 15 mm, 200 mm). The array of $d_{ee} = 1.8$ cm excels that of $d_{ee} = 2.4$ cm in the ability of the restraining grating lobes. And the restraining

ability shows a big dynamic range. That is to say that the grating-lobe level can be kept low even if the main focus deviates the z-axis. This is advantageous for the focused ultrasound treatment because the low grating-lobe level can avoid the impairing of normal tissue while treating a deep-seated tumor.

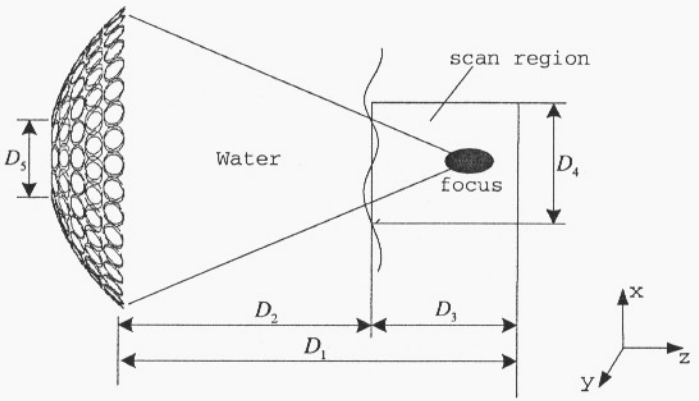

Fig. 1. Schematic of the HIFU scan scale.

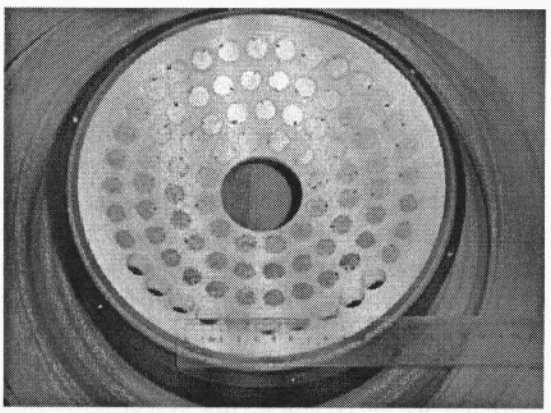

Fig. 2. Photograph of the inner holed spherical array.

Table 1. Treatment aims and optimization results.

Aims	Results
D_1 = 16 cm	Frequency f = 557 KHz
D_2 = 10 cm	Radius of spherical shell R = 20 cm
D_3 = 4 cm	Distance between elements d_{ee} = 1.8 cm
D_4 = 3 cm	Height of spherical shell = 3.2 cm
D_5 = 5 cm	Element number N = 96
A_1 = 43 W/cm^3	Diameter of element d_e = 1.4 cm
A_2 = 4 cm	Aperture of spherical shell = 17.4 cm
A_3 = 2, 3	Sound intensity gain [8] G = 65.05

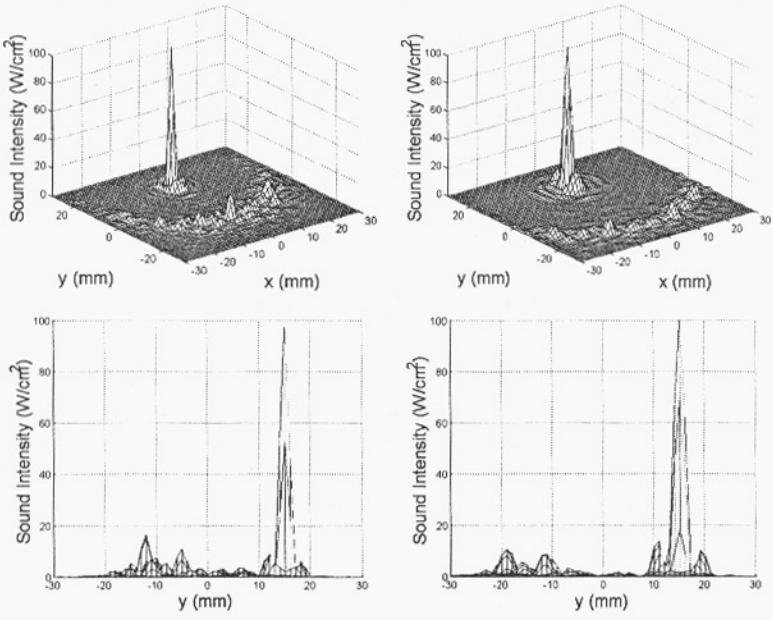

(a) dee = 2.4 cm (b) dee = 1.8 cm

Fig. 3. The grating lobes of the array when focus deviating z-axis.

Using the pseudo inverse method the driving signals have an amplitude and phase distribution shown in Fig. 4. The figures on the left-hand side are the amplitudes, and those on the right-hand side are phases. Using excitation optimizing algorithm amplitudes of the particle velocity for the phased-array elements are kept uniform and are below the maximum amplitude before the optimization. The phases of the particle velocity are kept invariant before and after the optimization and fluctuate within the range from $-\pi$ to $+\pi$.

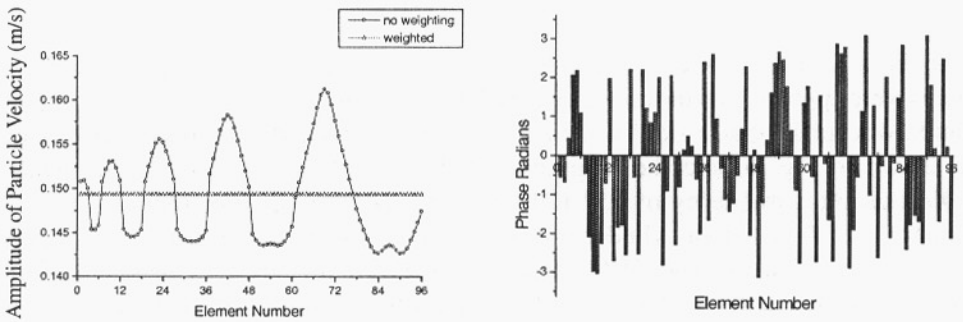

Fig. 4. Amplitude and phase distribution of particle velocity.

The optimization results show that different ratios of the distance between elements to the wavelength leads to different optimization results. Low frequency is preferred for reducing the element number. The optional radius of the spherical shell is not always the center of the scan scale, but tends to the largest depth of scan region. An optimal element aperture tends to the largest limit, which means that the element size is inverse proportionel to the element number. For the HIFU treatment the larger are D_1, D_2, A_1, the lower f and R are preferred.

4. Experimental device

The transducer array with 96 elements needs 96 channel driving signals of controlled phase and amplitude. Under this requirement, a phased signal driving system was developed based on FPGA. The system composed of five main parts is shown in Fig. 5. By a controlling computer and digital I/O card, each element can get the needed signal of different phase and amplitude in the procession of focusing.

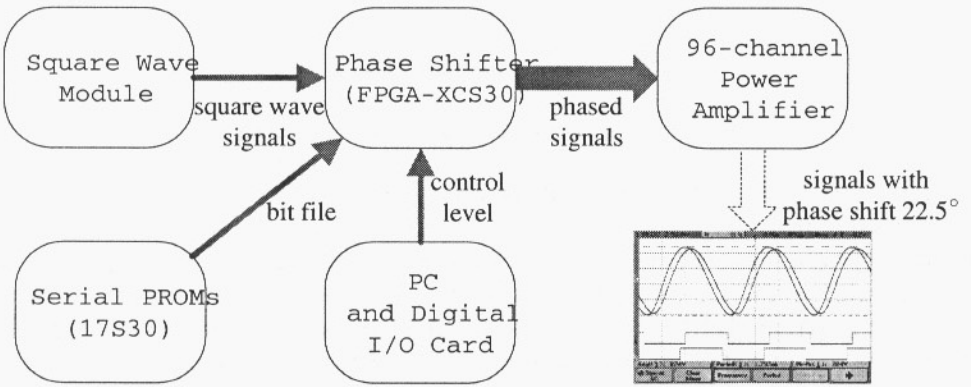

Fig. 5. Diagram of phased signal driving system.

In the experiments, 16 elements in the designed transducer array were used, and driving signals were applied from the above system. The phase shift of the driving system had 6-bit quantized accuracy that is $2\pi/2^6 = 0.0982$ (5.625°). Actual control phases of these elements are shown in Fig. 6, and the amplitude of the particle velocity for each element is 0.1493 m/s. At a frequency of 557 KHz the array could focus electronically in a 3 cm diameter, 10–16 cm depth cylinder region. Results compare the measured and simulated temperatures after a 6 seconds HIFU exposure, as shown in Table 2. In the scanning region four points included the nearest and farthest points in the radial and axial directions of the array. Their temperatures were measured by using the thermoelectric couples. The finite element software ANSYS 5.7 was applied to calculate the simulation results.

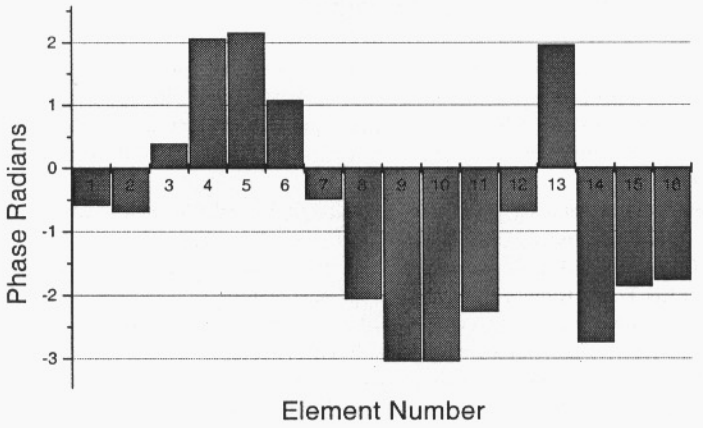

Fig. 6. Control phase distribution of 16 elements.

Table 2. Comparison of the simulation with measurement results.

Test points (cm)	Simulated results (°C)	Measured results (°C)
A (x=0, y=0, z=10)	70	69.1
B (x=0, y=0, z=16)	70	68.3
C (x=3, y=0, z=10)	70	67.5
D (x=3, y=0, z=16)	70	67.1

5. Conclusion

Basing on the Ebbini pseudo-inverse matrix and Penns bioheat transfer equation, an optimization method has been provided for the HIFU phased array. An inner holed spherical shell with 96 elements was designed for the HIFU treatment. The array could satisfy the need for a lower grating-lobe level and higher focal intensity gain to achieve the required therapeutic heating location. Ultrasound focusing experiments of the array using 16 elements had been carried out through a signal driving system based on FPGA, which could provide precise phased signals for the array elements. The results showed that the array could realize a large dynamic scan scale (3 cm diameter, 10–16 cm depth) with least elements. The design method of the phased array is useful and feasible for the HIFU device.

Acknowledgments

This work was supported by the grants 994419072 from the Shanghai Technological Development Foundation.

References

[1] D. R. Daum, K. Hynynen, *A 256-element ultrasonic phased array system for the treatment of large volumes of deep seated tissue,* IEEE Trans. Ultrason. Ferroelect. Freq. Contr., **46**, 5, 1254–1268 (1999).

[2] P. Van Baren, J. U. Kluiwstra, R. Seip, *et al., 2D large aperture ultrasound phased arrays for hyperthermia cancer therapy: design, fabrication and experimental results*, Proceedings of IEEE Ultrasonics Symposium, 1269–1272 (1995).

[3] S. Ginter, *Numerical simulation of ultrasound-thermotherapy combining nonlinear wave propagation with broadband soft-tissue absorption*, Ultrasonics, **37**, 10, 693–696 (2000).

[4] E. S. Ebbini, C. A. Cain, *A spherical-section ultrasound phased array applicator for deep localized hyperthermia*, IEEE Trans. Biomed. Eng., **38**, 7, 634–643 (1991).

[5] E. S. Ebbini, H. Wang, M. O'Dennell, *et al., Acoustic feedback for hyperthermia phased-array applicators: aberration correction, motion compensation and multiple focusing in the presence of tissue inhomogeneities*, Proceedings of IEEE Ultrasonics Symposium, 1343–1346 (1991).

[6] B. Y. Lu, W. L. Lin, Y. Y. Chen, *et al., A sixteen-channel phased array driving system for ultrasound hyperthermia*, Proceedings of the 19th Annual International Conference of the IEEE, 822–825 (1997).

[7] B. Y. Lu, W. L. Lin, Y. Y. Chen, *et al., A multifrequency driving system for ultrasound hyperthermia*, IEEE Engineering in Medicine and Biology Magazine, **18**, 5, 106–111 (1999).

[8] E. S. Ebbini, C. A. Cain, *Optimization of the intensity gain of multiple-focus phased-array heating patterns*, Int. J.Hyperthermia, **7**, 6, 953–973 (1991).

[9] H. H. Penns, *Analysis of tissue and arterial blood temperatures in the resting human forearm*, J. Applied Physiology, **1**, 1, 93–122 (1948).

[10] S. A. Goss, L. A. Frizzell, F. Dunn, *Ultrasonic absorption and attenuation in mammalian tissues*, Ultrasound Med. Biol., **5**, 1, 181–186 (1979).